Impact of frequency offsets and IQ imbalance on MC-CDMA reception based on channel tracking

François Horlin *Stefaan De Rore* *Eduardo Lopez-Estraviz*

Frederik Naessens *Liesbet Van der Perre*

Interuniversity Micro-Electronics Center (IMEC), Wireless Research

Kapeldreef 75, B-3001 Leuven, Belgium

E-mail : horlinf@imec.be

Submission date: April 1, 2005

Keywords:
- MC-CDMA
- Channel estimation error
- Synchronization errors
- Carrier frequency offset
- Clock frequency offset
- Front-end non-idealities
- IQ imbalance

Abstract

New air interfaces are currently being developed to meet the high spectral efficiency requirements of the emerging wireless communication systems. Multi-carrier code-division multiple access (MC-CDMA) is seen as a promising candidate for the fourth generation (4G) cellular communication systems because it can interestingly deal with the multipath propagation at a low processing complexity. Besides spectral efficiency and power consumption, the production cost of the transceiver should also be optimized. Direct conversion radio frequency (RF) receivers are appealing because they avoid costly intermediate frequency (IF) filters. However, they imply RF IQ separation, introducing a phase and amplitude mismatch between the I and Q branches. A communication system based on MC-CDMA is sensitive to synchronization errors and front-end non-idealities because it uses a long symbol duration. The goal of this paper is to evaluate the impact of the carrier frequency offset (CFO), the sampling clock offset (SCO) and the IQ imbalance on the MC-CDMA downlink system performance, considering a receiver based on channel tracking designed to cope with high mobility conditions. It is demonstrated that part of the effects is compensated by the channel estimation and an expression of the variance of the remaining symbol estimation error is provided. For the cellular system and the target performance considered in this paper, specifications are defined on the non-idealities. The results are validated with bit error rate (BER) simulations.

I. INTRODUCTION

Because of the limited frequency bandwidth, on the one hand, and the potential limited power of terminal stations, on the other hand, spectral and power efficiencies of future communication systems should be as high as possible. New air interfaces need to be developed to meet the new requirements. Cellular systems of the third generation (3G) are based on the recently emerged direct-sequence code-division multiple access (DS-CDMA) technique [1]. DS-CDMA offers a potentially high system capacity and interesting networking abilities. For example, soft hand-over can be supported between two cells making use of different codes at the base stations. However, the DS-CDMA system suffers from inter-symbol interference (ISI) and multi-user interference (MUI) caused by multi-path propagation, leading to a high loss of performance. The orthogonal frequency-division multiplexing (OFDM) modulation has been selected for wireless local area networks (WLANs) [2]. At the cost of the addition of a cyclic prefix, the time dispersive channel is seen in the frequency-domain as a set of parallel independent flat sub-channels and can be

equalized at a low complexity. Multi-carrier code-division multiple access (MC-CDMA) combines DS-CDMA and OFDM by applying the CDMA spreading on top of the channel equalized in the frequency domain, keeping the interesting orthogonality of the CDMA spreading codes [3], [4], [5]. Because it can deal with the multipath propagation at a low complexity, MC-CDMA is seen as a promising air interface for the fourth generation (4G) cellular communication systems.

On the other hand, integrated direct-conversion analog front-ends are now widely envisaged to replace the classical super-heterodyne structure because they avoid costly intermediate frequency (IF) filters [6]. Since the IQ demodulation is directly performed in the analog domain (rather than a first down-conversion to an intermediate frequency in the analog domain followed by an IQ demodulation in the digital domain), the system suffers from a phase and amplitude mismatch between the I and Q branches. Futhermore, because the filters and amplifiers on the I and Q branches are different, the transfer functions on the I and Q branches are also different. However, IQ imbalance is mostly frequency-independent for the small bandwidths considered in the actual cellular systems. It has been recently shown that IQ imbalance can be advantageously compensated digitally [7].

Though MC-CDMA is robust against the interference caused by the multipath propagation, it is sensitive to the system non-idealities that destroy the orthogonality between the carriers. Especially, the carrier frequency offset (CFO) and the sampling clock offset (SCO), caused by the local oscillators at the transmitter and receiver, and the IQ imbalance, caused by the use of direct-conversion analog front-ends, are destructive. In order to enable the communication in the presence of CFO, SCO and IQ imbalance, the digital receiver is generally structured in two steps. A rough estimation of the non-idealities is performed based on the transmission of a training sequence during the acquisition step taking place in front of the transmission of data. When data are transmitted, the non-idealities are pre-compensated according to the estimated values and the remaining error is tracked based on pilots that are inserted into the data symbols.

A lot of work relates to the acquisition of CFO and IQ imbalance. Because each of the two

effects destroys the estimation of the other effect, CFO and IQ imbalance need to be estimated together. Papers [8] and [9] introduce two different estimators of the CFO in the presence of IQ imbalance. While the estimator proposed in [8] is iterative and relies on a specifically designed pilot symbol in the frequency domain, the estimator proposed in [9] features a lower complexity and is compatible to the time-domain periodic training sequence imposed by the IEEE 802.11a WLAN standard. On the other hand, [10] proposes an estimator of the IQ imbalance in the presence of CFO. It exploits the fact that IQ imbalance destroys the smoothness of the propagation channels in the frequency domain. Interestingly, [11] proposes an integrated structure to compensate for the CFO and for frequency-dependent IQ imbalance. Finally, we also propose an integrated structure for joint CFO and IQ imbalance compensation taking the very strict specifications of the emerging 4G wireless systems into account [12].

When the CFO and IQ imbalance acquisition has been performed, the non-idealities can be pre-compensated and data symbols can be transmitted. However the remaining errors after the acquisition still cause a significant degradation of the MC-CDMA system performance. While [13] evaluates analytically the impact of CFO on the performance of a single-user MC-CDMA system, [14] and [15] extend the study of [13] to a multi-user MC-CDMA system. Interestingly, [16] demonstrates that the performance in the presence of CFO or SCO strongly degrades for an increasing number of carriers. Paper [16] studies also the effects of carrier phase jitter and timing jitter on the system. Because the CFO and SCO cause a phase rotation linearly increasing with the symbol index, the errors can be tracked based on the observation of the rotation on pilot symbols. An iterative method for tracking the CFO that maximizes the likelihood function is also proposed in [17]. Even if the impact of IQ imbalance on OFDM systems has already been investigated [10], the sensitivity of MC-CDMA systems to this effect is not yet studied.

In the present paper, the joint impact of CFO, SCO and IQ imbalance on the MC-CDMA downlink of a mobile communication system is assessed. Because the channels are time-varying, they need to be tracked for possible compensation [18], [19]. It is demonstrated that part of the er-

rors can be assimilated to the channel so that the channel estimation tracking system compensates partially for these effects.

The paper is organized as follows. Section II gives an overview of the system. In Section III, an equivalent matrix model of the CFO, SCO and IQ imbalance in the frequency domain is built. Based on the model, the error caused by the non-idealities at the output of a single-user detector is computed in Section IV. Because the considered detector relies on the tracking of the time-varying propagation channels, the impact of a channel estimation error on the detection performance is also evaluated. Finally, the channel estimation error is computed for the different non-idealities in Section V. The impact of the different non-idealities on the integrated system performance is evaluated numerically in Section VI.

In the sequel, the operator $\star$ denotes the convolution between two signals. $\mathrm{E}_x\left(f(x)\right)$ is the expectation of the function $f(x)$ over the random variable x. We use single- and double-underlined letters for the vectors and matrices respectively. Matrix $\underline{\underline{I}}_N$ is the identity matrix of size N and matrix $\underline{\underline{0}}_{M\times N}$ is a matrix of zeros of size $M \times N$. The operators $(.)^*$, $(.)^T$ and $(.)^H$ denote respectively the complex conjugate, transpose and hermitian transpose of a vector or a matrix. The trace of matrix $\underline{\underline{M}}$ is denoted by tr $\left[\underline{\underline{M}}\right]$. The operator $\otimes$ is the Kronecker product between two vectors or matrices.

II. System overview

The system under consideration is illustrated in Figure 1. At the base station, the different user symbol streams are spread with the CDMA codes and interleaved over the carriers. Frames of symbol blocks are formed, in which pilot blocks are inserted regularly. The frequency domain signal is transformed to the time domain by the use of an inverse Fourier transform (IFFT). An analog transmitter front-end is used at the base station to send the signals over the propagation channel. At the mobile terminal m ($m = 1, ..., M$), the signal is received through the receiver analog front-end. Because the mobile terminals are generally built at a lower cost than the base station, the non-idealities coming from the mobile terminal analog front-end are prevailing over

the ones coming from the base station. It is assumed that the mobile terminal front-end suffers from IQ imbalance. Furthermore, because one base station communicates simultaneously with multiple terminals, the crystal frequency of the base station is assumed to be the reference. The crystal at the mobile terminal generates CFO and SCO. The sampling time instant, CFO and IQ imbalance are generally acquired and pre-compensated before the detection of the symbols. An error is committed on the acquisition of all the effects. The impact of the remaining error on the MC-CDMA reception performance is studied. After going back to the frequency domain by the use of a fast Fourier transform (FFT), the received pilot symbols are separated from the received data symbols. The time-varying propagation channel is estimated based on each pilot symbol and time-interpolated between the pilot symbols. The user symbols are detected after inversion of the channel at each time instant, deinterleaving and CDMA despreading.

III. Model of the non-idealities in the frequency domain

The purpose of this section is to build an equivalent model of the CFO, SCO and IQ imbalance in the frequency domain. Figure 2 illustrates a simplified model of the non-idealities.

Each symbol $X(q)$ in the vector of symbols $\underline{X}$, defined as $\underline{X} := [X(-Q/2) \cdots X(Q/2-1)]^T$, is transmitted on the carrier frequency q by applying an IFFT on $\underline{X}$. The symbol block duration is equal to QT, where Q is the number of carriers and T is the duration of one symbol. Assuming that the vector of symbols is sent periodically (which is performed in practice by the addition of a cyclic prefix at the transmitter and by the removal of the corresponding samples at the receiver), the IFFT is equivalent to multiplying $X(q)$ by $\rho_q(t) = \frac{1}{\sqrt{Q}} e^{j2\pi qt/QT}$ and to summing the contributions on the different carriers. The baseband signal is up-converted to the carrier frequency ω_0, after low-pass filtering by $\psi_T(t)$ in order to remove the out-of-band components. The resulting signal $s_{RF}(t)$ is transmitted through a frequency selective channel $h_{RF}(t)$. Additive white Gaussian noise (AWGN) $w_{RF}(t)$, of one-sided power spectral density equal to N_0, is added in the first amplifier stages of the receiver front-end. The radio frequency (RF) received signal $r_{RF}(t)$ is finally down-converted to the baseband domain for complex operation, low-pass

filtered in order to avoid aliasing and sampled before going back to the frequency domain by the use of an FFT, corresponding to the multiplication of the received vector of samples by a matrix $\underline{\underline{F}} = \left[\frac{1}{\sqrt{Q}} e^{-jpq/Q}\right]_{p,q=-Q/2,\cdots,Q/2-1}$. The received vector is composed of the signals received on the different carrier frequencies, as defined in $\underline{Z} := [Z(-Q/2) \cdots Z(Q/2-1)]^T$. Due to the fact that the local oscillator at the receive terminal is different from the one at the transmit base-station, the down-conversion to the baseband domain is operated with a phase shift ϕ_0 and with a frequency shift $\Delta\omega$ (CFO), and the received signal is sampled with an initial phase t_0 different from 0 and with a period T' slightly different from the one at the transmitter T, $T' = T(1+\delta)$ (SCO). On the other hand, IQ imbalance caused by the use of different elements on the I and Q branches, is modeled by a difference in amplitude ϵ and phase $\Delta\phi$ between the two branches, and by the different low-pass filters $\psi_R^I(t)$ and $\psi_R^Q(t)$ on the two branches.

A. Impact of the receive front-end

If $r(t) := r_r(t) - j r_i(t)$ is the baseband representation of the RF received signal $r_{RF}(t)$, we have that

$$r_{RF}(t) \;=\; r_r(t)\cos(\omega_0 t) \;+\; r_i(t)\sin(\omega_0 t)\,. \tag{1}$$

Taking the CFO and IQ imbalance into account, the baseband component of the signal on the I branch after multiplication by the cosine is

$$y_r(t) \;=\; r_r(t)\,(1+\epsilon)\,\cos(\Delta\phi + \Delta\omega t + \phi_0) \;-\; r_i(t)\,(1+\epsilon)\,\sin(\Delta\phi + \Delta\omega t + \phi_0) \tag{2}$$

and the baseband component of the signal on the Q branch after multiplication by the sine is

$$y_i(t) \;=\; -r_r(t)\,(1-\epsilon)\,\sin(\Delta\phi - \Delta\omega t - \phi_0) \;+\; r_i(t)\,(1-\epsilon)\,\cos(\Delta\phi - \Delta\omega t - \phi_0)\,. \tag{3}$$

We are not interested in the high frequency components resulting from the multiplication with the cosine and sine because they will be later filtered out by the low-pass filters $\psi_R^I(t)$ and $\psi_R^Q(t)$. By defining $y(t) := y_r(t) - j y_i(t)$, we get that

$$y(t) \;=\; \alpha\, e^{-j(\Delta\omega t + \phi_0)}\, r(t) \;+\; \beta\, e^{j(\Delta\omega t + \phi_0)}\, r^*(t) \tag{4}$$

in which

$$\alpha := \cos(\Delta\phi) - j\epsilon\sin(\Delta\phi) \quad (5)$$

$$\beta := \epsilon\cos(\Delta\phi) + j\sin(\Delta\phi)\,. \quad (6)$$

The parameters α and β express the impact of the IQ imbalance on the received signal ($\alpha = 1$ and $\beta = 0$ when the two paths are exactly the same). The CFO leads to a frequency shift of the two components of the baseband received signal, as shown in (4).

If the IQ imbalance is frequency-independent, the low-pass filter is identical on the two I and Q branches so that $\psi_R(t) := \psi_R^I(t) = \psi_R^Q(t)$. We obtain

$$z(t) = y(t) \star \psi_R(t) \quad (7)$$

$$= \alpha\, e^{-j(\Delta\omega t+\phi_0)}\,(r(t)\star\psi_R(t)e^{j\Delta\omega t}) \,+\, \beta\, e^{j(\Delta\omega t+\phi_0)}\,(r(t)\star\psi_R(t)e^{j\Delta\omega t})^*\,. \quad (8)$$

The model is extended to the special case of frequency-dependent IQ imbalance in Appendix I.

B. Frequency domain transmission

Because the transmitted signal at the output of the IFFT is given by

$$x(t) \,=\, \frac{1}{\sqrt{Q}} \sum_{q=-Q/2}^{Q/2-1} X(q)\, e^{j\frac{2\pi qt}{QT}}\,, \quad (9)$$

based on (8), we have that

$$z(t) \,=\, \alpha\,\frac{1}{\sqrt{Q}} \sum_{q=-Q/2}^{Q/2-1} X(q)\, G(q)\, e^{j\frac{2\pi qt}{QT}}\, e^{-j(\Delta\omega t+\phi_0)}$$
$$+\, \beta\,\frac{1}{\sqrt{Q}} \sum_{q=-Q/2}^{Q/2-1} X^*(q)\, G^*(q)\, e^{-j\frac{2\pi qt}{QT}}\, e^{j(\Delta\omega t+\phi_0)} \,+\, w'(t) \quad (10)$$

in which $G(q)$ is the composite impulse response $g(t) := \psi_T(t) \star h(t) \star \psi_R(t)\, e^{j\Delta\omega t}$ at the carrier frequency q ($h(t)$ denotes the baseband represention of the RF channel $h_{RF}(t)$), and $w'(t)$ is the noise at the output of the received front-end, given by $w'(t) := \alpha\, e^{-j(\Delta\omega t+\phi_0)}\,(w(t)\star\psi_R(t)e^{j\Delta\omega t}) + \beta\, e^{j(\Delta\omega t+\phi_0)}\,(w(t)\star\psi_R(t)e^{j\Delta\omega t})^*$ ($w(t)$ denotes the baseband represention of the RF noise $w_{RF}(t)$).

After sampling, we get

$$z_s(n) := z(t \;=\; nT(1+\delta)+t_0) \tag{11}$$

$$= \alpha\,\frac{1}{\sqrt{Q}}\sum_{q=-Q/2}^{Q/2-1} X(q)\,G(q)\,e^{-j\,(\phi_0+\Delta\omega t_0)}e^{j\,\frac{2\pi t_0}{QT}q}\,e^{j(\frac{2\pi q}{Q}-\Delta\omega T)(1+\delta)n}$$

$$+\;\beta\,\frac{1}{\sqrt{Q}}\sum_{q=-Q/2}^{Q/2-1} X^*(q)\,G^*(q)\,e^{j\,(\phi_0+\Delta\omega t_0)}e^{-j\,\frac{2\pi t_0}{QT}q}\,e^{-j(\frac{2\pi q}{Q}-\Delta\omega T)(1+\delta)n}\;+\;w'_s(n) \tag{12}$$

where $w'_s(n) \;:=\; w'(t \;=\; nT(1+\delta)+t_0)$. Assuming that the filter $\psi_R(t)$ is a perfect low-pass filter of bandwidth $1/T'$, the noise samples are independent and of variance equal to $\sigma_w^2(t) = 2N_0/T'\dot{(}1+\epsilon^2) \simeq 2N_0/T'$.

C. Frequency domain reception

At the output of the FFT, the signal on each carrier p ($p = -Q/2, ..., Q/2-1$) is

$$Z(p) = \frac{1}{\sqrt{Q}}\sum_{n=-Q/2}^{Q/2-1} z_s(n)\,e^{-j\frac{2\pi np}{Q}} \tag{13}$$

$$= \alpha\sum_{q=-Q/2}^{Q/2-1} X(q)\,G(q)\,\gamma_0(q)\,\gamma(p,q)\;+\;\beta\sum_{q=Q/2}^{Q/2-1} X^*(q)\,G^*(q)\,\gamma_0^*(q)\,\gamma^*(-p,q)\;+\;W'(p) \tag{14}$$

in which $\gamma_0(q)$ and $\gamma(p,q)$ are given by

$$\gamma_0(q) \;:=\; e^{-j\,(\phi_0+\Delta\omega t_0)}\cdot e^{j\,\frac{2\pi t_0}{QT}q}\cdot e^{-j\left(\frac{\pi q\delta}{Q}-\frac{\Delta\omega T}{2}-\frac{\Delta\omega T\delta}{2}\right)}\cdot\frac{1}{Q}\,\frac{\sin\left(\pi q\delta-\frac{\Delta\omega QT}{2}-\frac{\Delta\omega QT\delta}{2}\right)}{\sin\left(\frac{\pi q\delta}{Q}-\frac{\Delta\omega T}{2}-\frac{\Delta\omega T\delta}{2}\right)} \tag{15}$$

$$\gamma(p,q) \;:=\; (-1)^{(q-p)}\cdot e^{-j\frac{\pi(q-p)}{Q}}\cdot\frac{1}{\cos(\frac{\pi(q-p)}{Q})\;+\;\left(\tan(\frac{\pi q\delta}{Q}-\frac{\Delta\omega T}{2}-\frac{\Delta\omega T\delta}{2})\right)^{-1}\sin(\frac{\pi(q-p)}{Q})} \tag{16}$$

and $W'(p) \;:=\; \frac{1}{\sqrt{Q}}\sum_{n=-Q/2}^{Q/2-1} w'_s(n)\,e^{-j\frac{2\pi np}{Q}}$ is the noise in the frequency domain. Equality (14) has been obtained by noting that $\sum_{n=0}^{Q-1} x^n \;=\; (1-x^Q)/(1-x)$. If $\delta << 1$ (which is always the case with a realistic front-end) and if $\pi\delta << \Delta\omega T$ (which is often the case with a realistic front-

end and realistic acquisition algorithms), $\gamma_0(q)$ and $\gamma(p,q)$ can be interestingly approximated by

$$\gamma_0(q) \simeq e^{-j(\phi_0+\Delta\omega t_0-\frac{\Delta\omega T}{2})}\dot{e}^{j\frac{2\pi t_0}{QT}q}.\frac{\sin\left(\frac{\Delta\omega QT}{2}\right)}{\frac{\Delta\omega QT}{2}} \quad (17)$$

$$\gamma(p,q) \simeq \frac{(-1)^{(q-p)}\dot{e}^{-j\frac{\pi(q-p)}{Q}}}{\cos(\frac{\pi(q-p)}{Q})-(\frac{\Delta\omega T}{2})^{-1}\,\sin(\frac{\pi(q-p)}{Q})}. \quad (18)$$

Equality (14) can be expressed in the following matricial model

$$\underline{Z} = \alpha\,\underline{\underline{\gamma}}\,\underline{\underline{\Lambda}}_0\,\underline{\underline{\Lambda}}_G\,\underline{X} + \beta\,\underline{\underline{\tilde{\gamma}}}^*\,\underline{\underline{\Lambda}}_0^*\,\underline{\underline{\Lambda}}_G^*\,\underline{X}^* + \underline{W'} \quad (19)$$

where the matrix $\underline{\underline{\gamma}}$ is equal to $\underline{\underline{\gamma}} := [\gamma(p,q)]_{p,q=0\cdots Q-1}$ and the matrix $\underline{\underline{\tilde{\gamma}}}$ is a flipped version of $\underline{\underline{\gamma}}$ (the rows corresponding to $p = -Q/2+1,\cdots,Q/2-1$ are flipped). The matrices $\underline{\underline{\Lambda}}_0$ and $\underline{\underline{\Lambda}}_G$ are diagonal. Matrix $\underline{\underline{\Lambda}}_0$ contains the elements $\gamma_0(q)$ on its diagonal. Matrix $\underline{\underline{\Lambda}}_G$ contains the channel coefficients $G(q)$ on its diagonal. The noise vector $\underline{W'}$ is equal to $\underline{W'} := [W'(-Q/2)\cdots W'(Q/2-1)]^T$.

CFO causes a common rotation as well an amplitude variation on all carriers (see the impact of ϕ_0 and $\Delta\omega$ in (17)). SCO causes a rotation proportional to the carrier number (see the impact of t_0 in (17)). Mainly CFO creates inter-carrier interference (ICI) (see (18)). IQ imbalance adds an image of the transmitted vector (complex conjugated and flipped) that interferes with the desired signal (see (19)).

IV. Impact of the non-idealities on the MC-CDMA reception

The MC-CDMA downlink communication system is illustrated in Figure 3. Each user m sends a vector of complex symbols $\underline{s}^m$ of size B ($m = 1,\cdots,M$). The symbols are assumed to be independent and of variance σ_s^2. As we have indicated in the introduction, MC-CDMA first performs classical DS-CDMA symbol spreading, followed by OFDM modulation, such that the information symbols are spread across the Q different subcarriers. With $Q = BN$ and N the spreading code length, the $Q \times B$ spreading matrix, $\underline{\underline{\theta}}^m := \underline{a}^m \otimes \underline{\underline{I}}_B$, in which $\underline{a}^m := [a^m[0]\ldots a^m[N-1]]^T$ is the m-th user's code vector, spreads each symbol on equally spaced carriers.

At the mobile receiver m, a single-user detector is assumed. The channel is inverted based on

its estimated value $\underline{\underline{\hat{\Lambda}}}_G$. The user signal is recovered after CDMA despreading. Based on (19), the estimated vector of symbols is

$$\underline{\hat{s}}^m \;=\; (\underline{\theta}^m)^H\, \underline{\underline{\hat{\Lambda}}}_G^{-1} \left[\alpha\, \underline{\gamma}\, \underline{\underline{\Lambda}}_0\, \underline{\underline{\Lambda}}_G\, \underline{\theta}\, \underline{s} \;+\; \beta\, \underline{\tilde{\gamma}}^*\, \underline{\underline{\Lambda}}_0^*\, \underline{\underline{\Lambda}}_G^*\, \underline{\theta}\, \underline{s}^* \;+\; \underline{W'}\right] \tag{20}$$

in which

$$\underline{s} \;:=\; \left[\begin{array}{ccc} (\underline{s}^1)^T & \cdots & (\underline{s}^M)^T \end{array}\right]^T \tag{21}$$

$$\underline{\underline{\theta}} \;:=\; \left[\begin{array}{ccc} \underline{\theta}^1 & \cdots & \underline{\theta}^M \end{array}\right]. \tag{22}$$

When the channel is estimated, part of the non-idealities is estimated together with the channel. Based on (19), it is clear that the parameter α and the matrix $\underline{\underline{\Lambda}}_0$ can be assimilated to the channel matrix $\underline{\underline{\Lambda}}_G$. Since front-end non-idealities and additive noise perturbate the channel estimation process, an error matrix $\underline{\underline{\Lambda}}_e$ is committed on the estimate. We have that

$$\hat{\Lambda}_G \;=\; \alpha\, \underline{\underline{\Lambda}}_0\, \underline{\underline{\Lambda}}_G \;+\; \underline{\underline{\Lambda}}_e\,. \tag{23}$$

By making a first order approximation, we further have that

$$\hat{\Lambda}_G^{-1} \;=\; \frac{1}{\alpha}\,(\underline{\underline{\Lambda}}_0\, \underline{\underline{\Lambda}}_G)^{-1} \;-\; \frac{1}{\alpha^2}\,(\underline{\underline{\Lambda}}_0\, \underline{\underline{\Lambda}}_G)^{-1}\, \underline{\underline{\Lambda}}_e\, (\underline{\underline{\Lambda}}_0\, \underline{\underline{\Lambda}}_G)^{-1}\,. \tag{24}$$

By defining the matrices

$$\underline{\underline{\chi}} \;:=\; (\underline{\underline{\Lambda}}_0\, \underline{\underline{\Lambda}}_G)^{-1}\, \underline{\underline{\gamma}}\, (\underline{\underline{\Lambda}}_0\, \underline{\underline{\Lambda}}_G) \tag{25}$$

$$\underline{\underline{\chi}}_{iq} \;:=\; (\underline{\underline{\Lambda}}_0\, \underline{\underline{\Lambda}}_G)^{-1}\, \underline{\tilde{\gamma}}^*\, (\underline{\underline{\Lambda}}_0\, \underline{\underline{\Lambda}}_G)^*\,, \tag{26}$$

the average mean square error (MSE) is equal to

$$\bar{\sigma}^2 \;=\; \frac{1}{B}\,\mathrm{tr}\left[\mathrm{E}_{s,w,e}\left((\underline{\hat{s}}^m - \underline{s}^m)\,(\underline{\hat{s}}^m - \underline{s}^m)^H\right)\right] \tag{27}$$

$$\simeq\; \bar{\sigma}^2_{ns} \;+\; \bar{\sigma}^2_{offs} \;+\; \bar{\sigma}^2_{iq} \;+\; \bar{\sigma}^2_{ce} \tag{28}$$

in which

$$\bar{\sigma}^2_{ns} = \frac{\sigma^2_w}{B}\,\mathrm{tr}\left[(\underline{\underline{\theta}}^m)^H\left((\underline{\underline{\Lambda}}_0\,\underline{\underline{\Lambda}}_G)^H\,\underline{\underline{\Lambda}}_0\,\underline{\underline{\Lambda}}_G\right)^{-1}\underline{\underline{\theta}}^m\right] \tag{29}$$

$$\bar{\sigma}^2_{offs} = \frac{\sigma^2_s}{B}\,\mathrm{tr}\left[(\underline{\underline{\theta}}^m)^H\left(\underline{\underline{\chi}}\,\underline{\underline{\theta}}\,\underline{\underline{\theta}}^H\,\underline{\underline{\chi}}^H - 2\Re(\underline{\underline{\chi}}) + \underline{\underline{I}}_Q\right)\underline{\underline{\theta}}^m\right] \tag{30}$$

$$\bar{\sigma}^2_{iq} = \frac{\sigma^2_s}{B}\left|\frac{\beta}{\alpha}\right|^2\,\mathrm{tr}\left[(\underline{\underline{\theta}}^m)^H\left(\underline{\underline{\chi}}_{iq}\,\underline{\underline{\theta}}\,\underline{\underline{\theta}}^H\,\underline{\underline{\chi}}^H_{iq}\right)\underline{\underline{\theta}}^m\right] \tag{31}$$

$$\bar{\sigma}^2_{ce} = \frac{\sigma^2_s}{B|\alpha|^2}\,\mathrm{tr}\left[\underline{\underline{\theta}}^H\underline{\underline{\chi}}^H(\underline{\underline{\Lambda}}_0\underline{\underline{\Lambda}}_G)^{-H}\,\mathrm{E}_e\left(\underline{\underline{\Lambda}}^H_e\,\underline{\underline{\theta}}^m(\underline{\underline{\theta}}^m)^H\underline{\underline{\Lambda}}_e\right)\,(\underline{\underline{\Lambda}}_0\underline{\underline{\Lambda}}_G)^{-1}\underline{\underline{\chi}}\,\underline{\underline{\theta}}\right]\,. \tag{32}$$

The terms (29), (30), (31) and (32) denote respectively the contributions of the additive noise, frequency offsets, IQ imbalance and channel estimation. Two MSE terms coming jointly from IQ imbalance/noise and channel estimation have been neglected since they are of the second order. Note that the contributions of the non-diagonal terms of $\underline{\underline{\chi}}$ in $\bar{\sigma}^2_{ce}$ and of the flipped version of $\underline{\underline{\chi}}_{iq}$ in $\bar{\sigma}^2_{iq}$ are also of the second order. The mathematical derivations leading to (29), (30), (31) and (32) can be found in Appendix II.

The last MSE term (32) depends on the second order statistics of the channel estimation error. In the next section, the channel estimation error auto-correlation matrix is computed by taking the CFO, SCO and IQ imbalance into account.

V. Impact of the non-idealities on the channel estimation

In Figure 4, the channel estimator proposed in [20] is represented. It is based on the transmission of one OFDM binary pilot symbol $\underline{X}_p$ of size Q at the base station and on the maximum-likelihood (ML) estimation of the time domain channel impulse response at the mobile terminal (note that it is possible to restrict the pilot symbol to a limited set of carriers).

At the receiver, part of the front-end non-idealities is estimated together with the channel. Especially the IQ coefficient α and the frequency offset coefficients $\gamma_0(q)$ are assimilated to the channel coefficients $G(q)$. In the frequency domain, the estimated composite channel is

$$\underline{G_0} \;=\; \alpha\,\underline{\underline{\Lambda}}_0\,\underline{G} \tag{33}$$

in which $\underline{G} \;:=\; [G(-Q/2)\cdots G(Q/2-1)]^T$.

Under the assumption that the channel is of finite order L (smaller than or equal to the cyclic prefix length), it is more efficient to estimate the channel in the time domain (L coefficients need to be estimated) than in the frequency domain (Q coefficients need to be estimated). By doing so, the correlation of the channel coefficients in the frequency domain is exploited. The channel in the frequency domain is the non-normalized FFT of the channel in the time domain, as expressed in

$$\underline{G_0} \;=\; \underline{\underline{\bar{F}}}\,\underline{g_0} \tag{34}$$

where $\underline{g_0}$ is the channel $\underline{G_0}$ in the time domain and $\underline{\underline{\bar{F}}}$ is a matrix of size $Q \times L$ composed of the L first columns of the square matrix $\sqrt{Q} \cdot \underline{\underline{F}}$ of size Q.

The ML channel estimator first performs an initial frequency domain channel estimate by inverting the pilot coefficients (multiplication of the received vector $\underline{Z}$ by the diagonal matrix $\underline{\underline{\Lambda}}_p$ composed of the pilot coefficients $\underline{X}_p$), and then transforms the initial estimate to the time domain estimate $\underline{\hat{g}}$ (multiplication of the result by the matrix $\underline{\underline{\bar{F}}}^H$) [20]. Finally, the estimate in the frequency domain $\underline{\hat{G}}$ is obtained by multiplying the result by $\underline{\underline{\bar{F}}}$.

Based on (19), the estimated channel is

$$\underline{\hat{G}} \;=\; \frac{1}{Q}\,\underline{\underline{\bar{F}}}\,\underline{\underline{\bar{F}}}^H\,\underline{\underline{\Lambda}}_p^H\left[\underline{\underline{\gamma}}\,\underline{\underline{\Lambda}}_p\,\underline{\underline{\bar{F}}}\,\underline{g_0} \;+\; \frac{\beta}{\alpha^*}\,\underline{\underline{\tilde{\gamma}}}^*\,\underline{\underline{\Lambda}}_p^*\,\underline{\underline{\bar{F}}}^*\,\underline{g_0^*} \;+\; \underline{W'}\right]. \tag{35}$$

By defining the matrices

$$\underline{\underline{\chi}}_{ce} \;:=\; \underline{\underline{\Lambda}}_p^H\,\underline{\underline{\gamma}}\,\underline{\underline{\Lambda}}_p \tag{36}$$

$$\underline{\underline{\chi}}_{ce,iq} \;:=\; \underline{\underline{\Lambda}}_p^H\,\underline{\underline{\tilde{\gamma}}}^*\,\underline{\underline{\Lambda}}_p^*, \tag{37}$$

the channel estimate error auto-correlation matrix is

$$\underline{\underline{R}}_{ce} \;=\; \mathrm{E}_{g,w}\left((\underline{\hat{G}} - \underline{G_0})\,(\underline{\hat{G}} - \underline{G_0})^H\right) \tag{38}$$

$$\;=\; \underline{\underline{R}}_{ce,ns} \;+\; \underline{\underline{R}}_{ce,offs} \;+\; \underline{\underline{R}}_{ce,iq} \tag{39}$$

in which

$$\underline{\underline{R}}_{ce,ns} = \frac{\sigma_w^2}{Q}\,\underline{\underline{\bar{F}}}\,\underline{\underline{\bar{F}}}^H \tag{40}$$

$$\underline{\underline{R}}_{ce,offs} = \frac{1}{Q^2}\,\underline{\underline{\bar{F}}}\,\underline{\underline{\bar{F}}}^H\,(\underline{\underline{\chi}}_{ce} - \underline{\underline{I}}_Q)\,\underline{\underline{\bar{F}}}\cdot \mathrm{E}_g\left(\underline{g}_0\,\underline{g}_0^H\right)\cdot \underline{\underline{\bar{F}}}^H\,(\underline{\underline{\chi}}_{ce} - \underline{\underline{I}}_Q)^H\,\underline{\underline{\bar{F}}}\,\underline{\underline{\bar{F}}}^H \tag{41}$$

$$\underline{\underline{R}}_{ce,iq} = \frac{1}{Q^2}\left|\frac{\beta}{\alpha}\right|^2\,\underline{\underline{\bar{F}}}\,\underline{\underline{\bar{F}}}^H\,\underline{\underline{\chi}}_{ce,iq}\,\underline{\underline{\bar{F}}}^*\cdot \mathrm{E}_g\left(\underline{g}_0^*\,\underline{g}_0^T\right)\cdot \underline{\underline{\bar{F}}}^T\,\underline{\underline{\chi}}_{ce,iq}^H\,\underline{\underline{\bar{F}}}\,\underline{\underline{\bar{F}}}^H\,. \tag{42}$$

The terms (40), (41) and (42) denote respectively the contributions of the additive noise, frequency offsets and IQ imbalance. It is assumed that the channel taps are independent and with complex coefficients of the same variance (the real and imaginary parts of each tap have an identical variance). The mathematical derivations leading to (40), (41) and (42) can be found in Appendix III.

In the absence of non-idealities, the average estimation error variance is equal to $1/Q$ tr $\left[\underline{\underline{R}}_{ce,ns}\right] = \sigma_w^2 L/Q$. Thanks to the fact that the channels have been estimated in the time domain, an interesting decrease of the error variance by a factor L/Q is observed.

VI. Numerical results

A. System under consideration

We consider a mobile cellular system, which operates in an outdoor sub-urban macro-cell propagation environment. The channel model is largely inspired from the 3GPP TR25.996 geometrical spatial channel model [21]. The radius of the cell is equal to 3 km. The mobile terminals are moving at a speed ranging from 0 (static) to 120 km/h (highly mobile). The system operates at a carrier frequency of 2 GHz, with a system bandwidth of 5 MHz. The performance (MSE or bit error rate (BER)) is averaged over 100 stochastic channel realizations. The performance is determined as a function of the transmit power at the base station, or, equivalently, as a function of the received symbol energy averaged over the channel realizations.

The user signals are spread by periodic Walsh-Hadamard codes for spreading, which are overlaid with an aperiodic Gold code for scrambling. A spreading factor equal to 8 has been chosen. The system is fully loaded, so that 8 users are active . QPSK, 16QAM, or 64QAM constellation is used with $Q = 128$ sub-channels, and a CP length of $L = 32$. Both at the transmitter and at the

receiver, the signal is shaped by a half-root Nyquist filter. The roll-off factor is equal to 0.2. The channel is estimated every 5 symbol blocks based on a full pilot symbol block and is interpolated between two estimates. The pilot symbol is a truncated pseudo-noise sequence. Because CFO and SCO mainly cause a rotation on the different carriers, the polar interpolation has been selected. No channel coding has been applied in order to not hide the effects of the front-end.

B. Specifications on CFO, SCO and IQ imbalance

Our goal is to define specifications on the CFO, SCO and IQ imbalance based on the analytical expressions of the MSE (30), (31), (41) and (42). The acquisition algorithms need to be designed to meet the CFO and IQ imbalance specifications. The crystal oscillator needs to respect the SCO specification. As an example, we target an average signal-to-noise ratio (SNR) flooring at 25 dB due to the CFO/SCO and IQ imbalance separately (22 dB if the effects are combined). This is clearly sufficient to support QPSK and 16QAM, but certainly not to support 64QAM (see the BER curves of the AWGN channel illustrated in Figure 9 for each constellation).

The impact of CFO on the MSE is presented in Figure 5 for different values of the SCO. The CFO ranges up to 10 kHz (this corresponds to the performance of extremely bad CFO acquisition algorithms) and the SCO ranges up to 100 ppm (this corresponds to poorly designed crystal oscillators). The solid curves represent the impact of CFO/SCO on the single-user detector (term (30)) and the dashed curves represent the impact of channel estimation errors due to CFO/SCO on the single-user detector (term (41) inserted in (32)). To the first order of approximation, the other MSE terms are independent on the CFO/SCO. The MSE increases linearly with the CFO and SCO values. The impact of CFO and SCO on single-user detection is prevailing over the one of channel estimation errors due to CFO and SCO. To achieve 25 dB average SNR, the SCO is not critical. On the other hand, the CFO should be limited to 1 kHz.

On the other hand, the impact of IQ imbalance on the MSE is shown in Figure 6. Because the bandwidth of the system is small, we consider that the IQ imbalance is frequency-independent. As an upper-bound on the range, we select an IQ amplitude mismatch of 10% and an IQ phase

mismatch of 10% of 2π (this corresponds to the specifications of a poorly designed quadrature frequency down-converter in the absence of IQ imbalance acquisition). The solid curves represent the impact of IQ imbalance on the single-user detector (term (31)) and the dashed curves represent the impact of channel estimation errors due to IQ imbalance on the single-user detector (term (42) inserted in (32)). To the first order of approximation, the other MSE terms are independent on the IQ imbalance. The MSE increases rapidly with the IQ imbalance so that IQ can become dominant over the other effects. Again, the impact of IQ imbalance on single-user detection is prevailing over the one of channel estimation errors due to IQ imbalance. To achieve 25 dB average SNR, the IQ amplitude mismatch should be limited to 2.5% and the IQ phase mismatch should be limited to 1^o.

Finally the output SNR is illustrated in Figure 7 as a function of the ratio E_s/N_0 (E_s denotes the average received symbol energy and N_0 denotes the noise one-sided power spectral density). The non-idealities are settled at their specification value: 1 kHz CFO, 100 ppm SCO, 2.5% IQ amplitude mismatch and 1^o IQ phase mismatch. The solid curves represent the impact of additive noise, CFO/SCO and IQ imbalance on the performance of the single-user detector (terms (29), (30) and (31)). The dashed curves represent the impact of the channel estimation errors due to additive noise, CFO/SCO and IQ imbalance on the performance of the single-user detector (terms (40), (41) and (42) inserted in the term (32)). While at low values of E_s/N_0, the noise is dominant over the CFO, SCO and IQ imbalance, the SNR floors at 22 dB for high values of E_s/N_0. As foreseen, the average SNR floors at 25 dB due to CFO/SCO and IQ imbalance independently.

C. Final performance

The goal of the present sub-section is to validate the approach followed to define the system specifications with BER curves.

Figure 8 illustrates the performance of a static system using a 16QAM constellation. Each non-ideality is activated separately at its specification value. For a matter of comparison, the degradation due to phase noise (PN) is also illustrated. Typical values of the PN power and bandwidth

have been selected. The power is equal to 32 dBc and the bandwidth is equal to 200 kHz [22]. In the presence of all non-idealities, the BER floors at 3.10^{-4}. IQ imbalance has a stronger effect than CFO/SCO. The impact of PN is negligible with respect to the one of CFO/SCO and IQ imbalance.

Figure 9 illustrates the performance of a static system for each possible constellation. The performance of the ideal system (dashed curves) is compared to the performance of the system in the presence of the non-idealities (solid curves). All non-idealities are activated at their specifications. As foreseen, QPSK and 16QAM can be supported while 64QAM suffers from a too high degradation (considering that a BER higher than 10^{-3} is not sufficient).

Figure 10 illustrates the performance of a mobile system using a QPSK constellation. The performance of a static system is compared to the performance of a system in which the terminal moves at a pedestrian speed (10 km/h), at a low vehicular speed (60 km/h) and at a high vehicular speed (120 km/h). Both the performance of the ideal system (dashed curves) and the performance of the system in the presence of the non-idealities (solid curves) degrade significantly for an increasing speed. However, it is shown that a system employing a QPSK constellation can reach an acceptable BER equal to 4.10^{-4} at high vehicular speeds.

VII. Conclusion

In this paper, the impact of synchronization errors (CFO, SCO) and of front-end non-idealities (IQ imbalance) on the reception of a MC-CDMA downlink signal has been studied. A single-user detector, that successively inverts the propagation channel in the frequency domain and correlates the resulting estimated chip sequence with the terminal CDMA code, has been assumed. Because mobile environments are targeted, we have assumed that the time-varying channels are estimated regularly using the ML channel estimation scheme based on pilot symbols, and time-interpolated between the pilots. It has been demonstrated that the tracking of the channel compensates for part of the non-idealities, and an analytical expression of the remaining symbol estimation error variance has been derived. The impact of the channel estimation errors on the final performance is negligible with respect to the one of the noise and of the non-idealities. The SNR at the output

of the resulting receiver decreases linearly with the CFO and SCO. For the cellular system and the target performance under consideration, the SCO is negligible with respect to the CFO. On the other hand, the performance of the system degrades very fast with the IQ imbalance, which can become rapidly the limiting factor.

APPENDIX I: MODEL OF THE FREQUENCY-DEPENDENT IQ IMBALANCE

The goal of this appendix is to extend the frequency domain model of the non-idealities to frequency-dependent IQ imbalance. In case of frequency-dependent IQ imbalance, the low-pass filters on the I and Q branches are different. The signal $y_r(t)$ in (2) filtered out by the low-pass filter $\psi_R^I(t)$ is given by

$$\begin{aligned} z_r(t) &= \frac{1}{2}(1+\epsilon)\,(\cos(\Delta\phi) + j\sin(\Delta\phi))\,\left(\psi_R^I(t) \star e^{j(\Delta\omega t+\phi_0)}\, r^*(t)\right) \\ &+ \frac{1}{2}(1+\epsilon)\,(\cos(\Delta\phi) - j\sin(\Delta\phi))\,\left(\psi_R^I(t) \star e^{-j(\Delta\omega t+\phi_0)}\, r(t)\right) \end{aligned} \tag{43}$$

and the signal $y_i(t)$ in (3) filtered out by the low-pass filter $\psi_R^Q(t)$ is given by

$$\begin{aligned} z_i(t) &= j\frac{1}{2}(1-\epsilon)\,(\cos(\Delta\phi) + j\sin(\Delta\phi))\,\left(\psi_R^Q(t) \star e^{-j(\Delta\omega t+\phi_0)}\, r(t)\right) \\ &- j\frac{1}{2}(1-\epsilon)\,(\cos(\Delta\phi) - j\sin(\Delta\phi))\,\left(\psi_R^Q(t) \star e^{j(\Delta\omega t+\phi_0)}\, r^*(t)\right). \end{aligned} \tag{44}$$

By defining $z(t) := z_r(t) - jz_i(t)$, we get that

$$\begin{aligned} z(t) &= e^{-j(\Delta\omega t+\phi_0)}\,\left(r(t) \star (\alpha\psi_R(t)e^{j\Delta\omega t} + \beta^*\epsilon_R(t)e^{j\Delta\omega t})\right) \\ &+ e^{j(\Delta\omega t+\phi_0)}\,\left(r(t) \star (\beta^*\psi_R(t)e^{j\Delta\omega t} + \alpha\epsilon_R(t)e^{j\Delta\omega t})\right)^* \end{aligned} \tag{45}$$

in which α and β, defined in (5) and (6), denote the IQ imbalance generated by the local oscillator, and

$$\begin{aligned} \psi_R(t) &:= (\psi_R^I(t) + \psi_R^Q(t))/2 \\ \epsilon_R(t) &:= (\psi_R^I(t) - \psi_R^Q(t))/2 \end{aligned} \tag{46}$$

denote the average low-pass filter and the impulse response mismatch respectively. The final model (19) can be easily adapted to

$$\underline{Z} = \underline{\gamma}\,\underline{\underline{\Lambda}}_0\,\underline{\underline{\Lambda}}_{G,\alpha}\,\underline{X} + \underline{\tilde{\gamma}}^*\,\underline{\underline{\Lambda}}_0^*\,\underline{\underline{\Lambda}}_{G,\beta}^*\,\underline{X}^* + \underline{W'} \tag{47}$$

in which $\underline{\underline{\Lambda}}_{G,\alpha}$ is a diagonal matrix containing the composite impulse response $g(t) := \psi_T(t) \star h(t) \star (\alpha\psi_R(t)e^{j\Delta\omega t} + \beta^*\epsilon_R(t)e^{j\Delta\omega t})$ in the frequency domain on its diagonal, and $\underline{\underline{\Lambda}}_{G,\beta}$ is a diagonal matrix containing the composite impulse response $g(t) := \psi_T(t)\star h(t)\star(\beta^*\psi_R(t)e^{j\Delta\omega t} + \alpha\epsilon_R(t)e^{j\Delta\omega t})$ in the frequency domain on its diagonal. The symbol MSE and the channel estimation MSE can be computed based on the model (47), leading to (28) and (39) in which the products $\alpha\,\underline{\underline{\Lambda}}_G$ and $\beta\,\underline{\underline{\Lambda}}_G^*$ are replaced by $\underline{\underline{\Lambda}}_{G,\alpha}$ and $\underline{\underline{\Lambda}}_{G,\beta}^*$.

APPENDIX II: DERIVATION OF SYMBOL ESTIMATION MSE

The goal of this appendix is to derive the expressions (29), (30), (31) and (32).

Starting from the expression of the symbol estimate (20), and relying on the definitions (25) and (26), the symbol estimation error is given by

$$\begin{aligned}
\underline{\hat{s}}^m - \underline{s}^m &= (\underline{\underline{\theta}}^m)^H \left(\underline{\underline{\chi}} - \underline{\underline{I}}_Q\right) \underline{\underline{\theta}}\,\underline{s} - \frac{1}{\alpha}\,(\underline{\underline{\theta}}^m)^H \left(\underline{\underline{\Lambda}}_0\,\underline{\underline{\Lambda}}_G\right)^{-1} \underline{\underline{\Lambda}}_e\,\underline{\underline{\chi}}\,\underline{\underline{\theta}}\,\underline{s} \\
&+ \frac{\beta}{\alpha}\,(\underline{\underline{\theta}}^m)^H\,\underline{\underline{\chi}}_{iq}\,\underline{\underline{\theta}}\,\underline{s}^* - \frac{\beta}{\alpha^2}\,(\underline{\underline{\theta}}^m)^H \left(\underline{\underline{\Lambda}}_0\,\underline{\underline{\Lambda}}_G\right)^{-1} \underline{\underline{\Lambda}}_e\,\underline{\underline{\chi}}_{iq}\,\underline{\underline{\theta}}\,\underline{s}^* \\
&+ \frac{1}{\alpha}\,(\underline{\underline{\theta}}^m)^H \left(\underline{\underline{\Lambda}}_0\,\underline{\underline{\Lambda}}_G\right)^{-1} \underline{W'} - \frac{1}{\alpha^2}\,(\underline{\underline{\theta}}^m)^H \left(\underline{\underline{\Lambda}}_0\,\underline{\underline{\Lambda}}_G\right)^{-1} \underline{\underline{\Lambda}}_e \left(\underline{\underline{\Lambda}}_0\,\underline{\underline{\Lambda}}_G\right)^{-1} \underline{W'},
\end{aligned} \tag{48}$$

obtained by noting that $\underline{s}^m = (\underline{\underline{\theta}}^m)^H\,\underline{\underline{\theta}}\,\underline{s}$.

The average MSE (27) is defined as the trace of the auto-correlation of the symbol estimation error (48) divided by the number of symbols. It can be easily computed based on two facts:

- By making an approximation of the second order, the terms 4 and 6 in (48) can be neglected at high SNRs (they are generated by both the IQ imbalance/noise and the channel estimation error).
- The cross-correlation between two different terms in (48) is always equal to zero (remark that $\mathrm{E}_{s,w,e}\,(\underline{s}\,\underline{s}) = \underline{\underline{0}}_{BM\times BM}$ and that the mean of the symbol or noise or channel estimation error independently is equal to zero).

The noise term (29) is the auto-correlation of the term 5 in (48). The CFO/SCO term (30) is the auto-correlation of the term 1 in (48) (note also that $\underline{\underline{\theta}}\,\underline{\underline{\theta}}^H\,\underline{\underline{\theta}}^m = \underline{\underline{\theta}}^m$). The IQ imbalance term (31) is the auto-correlation of the term 3 in (48). The channel estimation term (32) is the auto-correlation of the term 2 in (48).

APPENDIX III: DERIVATION OF CHANNEL ESTIMATION ERROR AUTO-CORRELATION

The goal of this appendix is to derive the expressions (40), (41) and (42).

Starting from the expression of the channel estimate (35), and relying on the definitions (36) and (37), the channel estimation error is given by

$$\hat{\underline{G}} - \underline{G}_0 = \frac{1}{Q}\,\underline{\underline{\bar{F}}}\,\underline{\underline{\bar{F}}}^H \left(\underline{\underline{\chi}}_{ce} - \underline{\underline{I}}_Q\right) \underline{\underline{\bar{F}}}\,\underline{g}_0 + \frac{\beta}{\alpha^*}\,\frac{1}{Q}\,\underline{\underline{\bar{F}}}\,\underline{\underline{\bar{F}}}^H\,\underline{\underline{\chi}}_{ce,iq}\,\underline{\underline{\bar{F}}}^*\,\underline{g}_0^* + \frac{1}{Q}\,\underline{\underline{\bar{F}}}\,\underline{\underline{\bar{F}}}^H\,\underline{\underline{\Lambda}}_p^H\,\underline{W'}\,. \quad (49)$$

We are interested in the channel estimation error auto-correlation (38). If the channel taps are independent, of zero-mean and with complex coefficients of the same variance (the real and imaginary parts of each tap have an identical variance), the cross-correlation between two different terms in (49) is always equal to zero (remark that $\mathrm{E}_{g,w}\left(\underline{g}_0\,\underline{g}_0\right) = \underline{\underline{0}}_{L\times L}$). The noise term (40) is the auto-correlation of the term 3 in (49). The CFO/SCO term (41) is the auto-correlation of the term 1 in (49). The IQ imbalance term (42) is the auto-correlation of the term 2 in (49).

REFERENCES

[1] T. Ojanperä and R. Prasad, *Wideband CDMA for Third Generation Mobile Communications*, Artech House Publishers, 1998.

[2] R. van Nee, G. Awater, M. Morikura, H. Takanashi, M. Webster, and K.W. Halford, "New high-rate wireless LAN standards," *IEEE Communications Magazine*, vol. 37, no. 12, pp. 82–88, December 1999.

[3] N. Yee, J-P. Linnartz, and G. Fettweis, "Multicarrier CDMA in indoor wireless radio networks," in *IEEE Proceedings of PIMRC*, September 1993, vol. 1, pp. 109–113.

[4] K. Fazel, "Performance of cdma/ofdm for mobile communication system," in *IEEE Proceedings of ICUPC*, October 1993, vol. 2, pp. 975–979.

[5] S. Kaiser, "OFDM code-division multiplexing in fading channels," *IEEE Transactions on Communications*, vol. 50, no. 8, pp. 1266–1273, August 2002.

[6] A. A. Abidi, "Direct-conversion radio transceivers for digital communications," *IEEE Journal on Solid-State Circuits*, vol. 30, no. 12, pp. 1399–1410, December 1995.

[7] A. Tarighat, R. Bagheri, and A. H. Sayed, "Compensation schemes and performance analysis of IQ imbalances in OFDM receivers," *IEEE Transactions on Signal Processing*, vol. 53, no. 8, pp. 3257–3268, August 2005.

[8] S. Fouladifard and H. Shafiee, "Frequency offset estimation in OFDM systems in presence of IQ imbalance," in *IEEE Proceedings of ICC*, May 2003, vol. 3, pp. 2071–2075.

[9] F. Yan, W-P. Zhu, and M. Omair Ahmad, "Carrier frequency offset estimation for OFDM systems with I/Q imbalance," in *IEEE Proceedings of 47th International Midwest Symposium on Circuits and Systems*, July 2004, vol. 2, pp. 633–636.

[10] J. Tubbax, B. Come, L. Van der Perre, S. Donnay, M. Engels, M. Moonen, and H. De Man, "Joint compensation of IQ imbalance and frequency offset in OFDM systems," in *IEEE Proceedings of Radio Wireless Conference*, August 2003, pp. 39–42.

[11] G. Xing, M. Shen, and H. Liu, "Frequency offset and I/Q imbalance compensation for direct-conversion receivers," *IEEE Transactions on Wireless Communications*, vol. 4, no. 2, pp. 673–680, March 2005.

[12] S. De Rore, E. Lopez-Estraviz, F. Horlin, and L. Van der Perre, "Joint estimation of carrier frequency offset and IQ imbalance for 4G mobile wireless systems," in *ICC 2006*, submitted.

[13] L. Tomba and W. A. Krzymien, "Sensitivity of the MC-CDMA access scheme to carrier phase noise and frequency offset," *IEEE Transactions on Vehicular Technology*, vol. 48, no. 5, pp. 1657–1665, September 1999.

[14] J. Jang and K. B. Lee, "Effects of frequency offset on MC/CDMA system performance," *IEEE Communications Letters*, vol. 3, no. 7, pp. 196–198, July 1999.

[15] Y. Kim, K. Bang, S. Choi, C. You, and D. Hong, "Effect of carrier frequency offset on performance of MC-CDMA systems," *IEEE Electronic Letters*, vol. 35, no. 5, pp. 378–379, March 1999.

[16] H. Steendam and M. Moeneclaey, "The effect of synchronization errors on MC-CDMA performance," in *IEEE Proceedings of ICC*, June 1999, pp. 1510–1514.

[17] Q. Tian and K. B. Letaief, "ML estimation and correction of frequency offset for MC-CDMA systems over fading channels," in *IEEE Proceedings of VTC Spring*, May 2001, vol. 1, pp. 571–575.

[18] S. Kaiser and P. Hoeher, "Performance of multi-carrier CDMA system with channel estimation in two dimensions," in *IEEE Proceedings of PIMRC*, September 1997, vol. 1, pp. 115–119.

[19] J. Choi, "Channel estimation for coherent multi-carrier CDMA systems over fast-fading channels," in *IEEE Proceedings of VTC*, May 2000, vol. 1, pp. 400–404.

[20] L. Deneire, P. Vandenameele, L. Van der Perre, B. Gyselinkx, and M. Engels, "A low-complexity ML channel estimator for OFDM," *IEEE Transactions on Communications*, vol. 51, no. 2, pp. 135–140, February 2003.

[21] 3GPP Technical specification group, "Tr25.996 v6.1.0, spatial channel model for multiple input multiple output (MIMO) simulations," September 2003.

[22] I. Vassiliou and et all, "A single-chip digitally calibrated 5.15-5.825-ghz 0.18-μm cmos transceiver for 802.11a wireless lan," *IEEE Journal on Solid-State Circuits*, vol. 38, no. 12, pp. 2221–2231, December 2003.

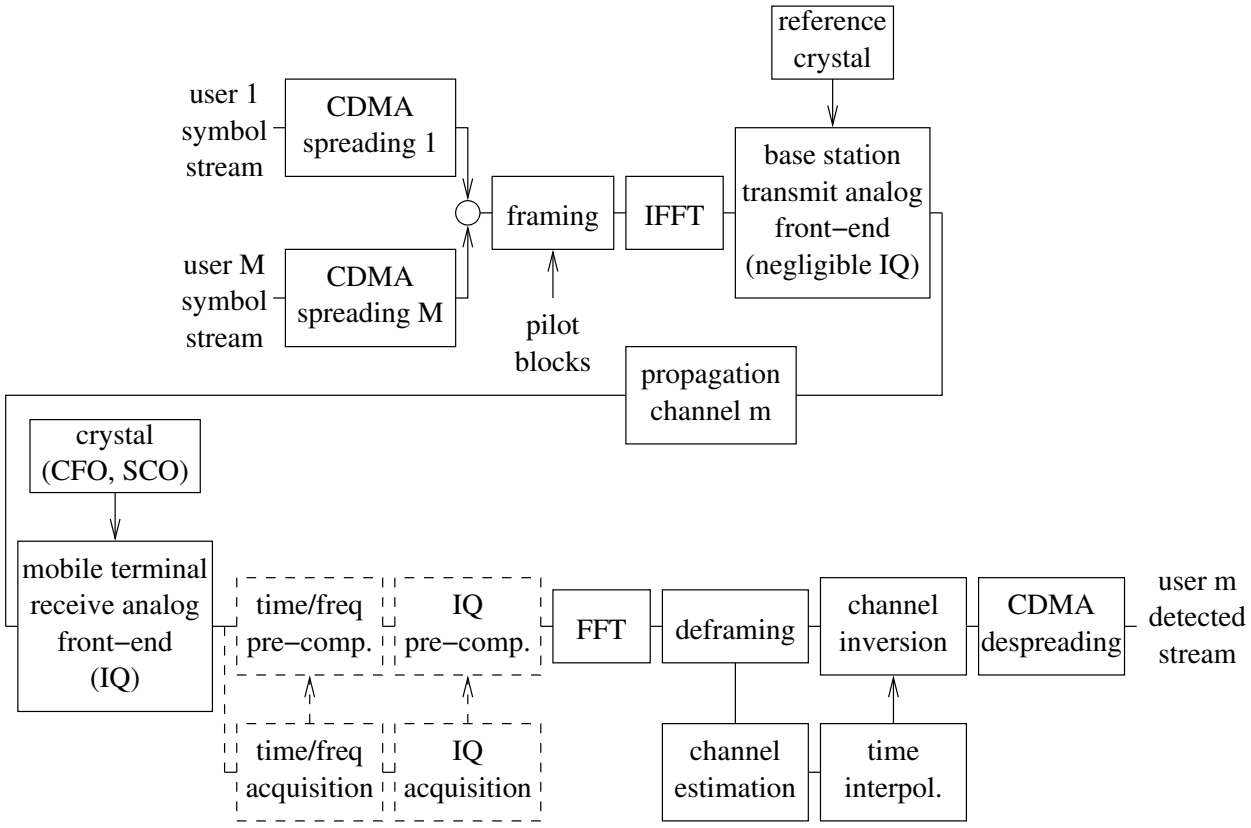

Fig. 1. Overall system model (dashed blocks are not considered in this study).

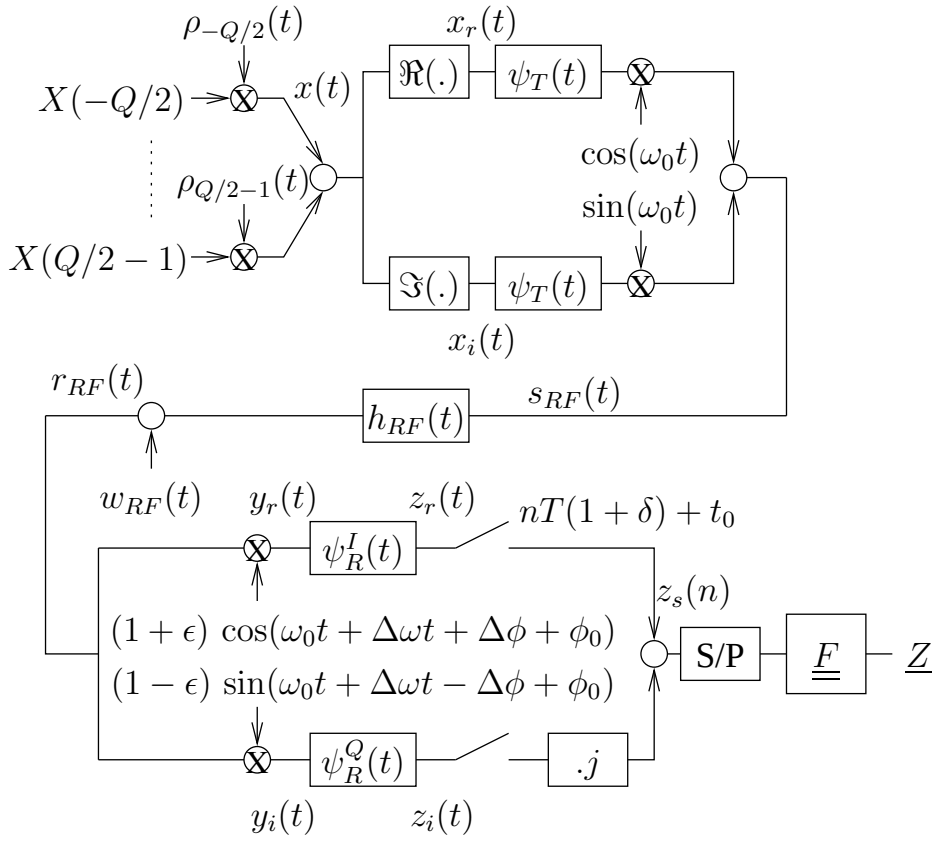

Fig. 2. Model of the non-idealities.

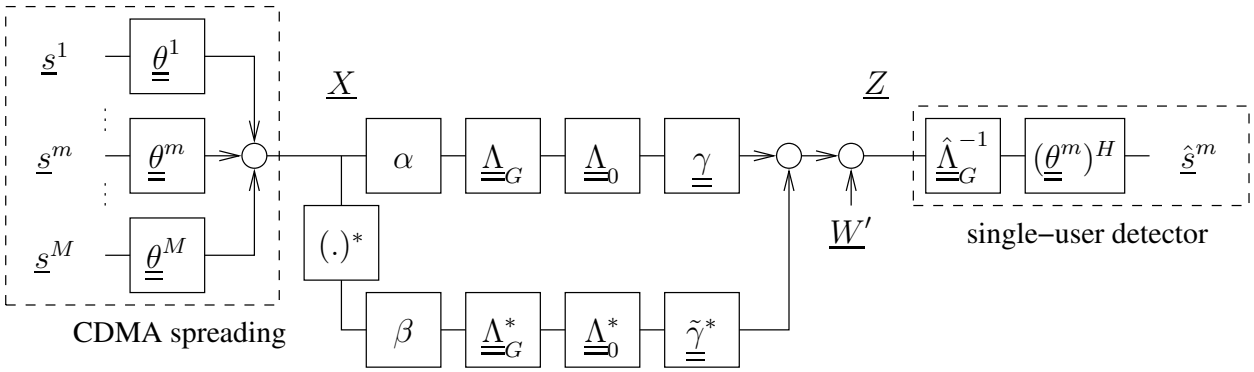

Fig. 3. MC-CDMA transceiver.

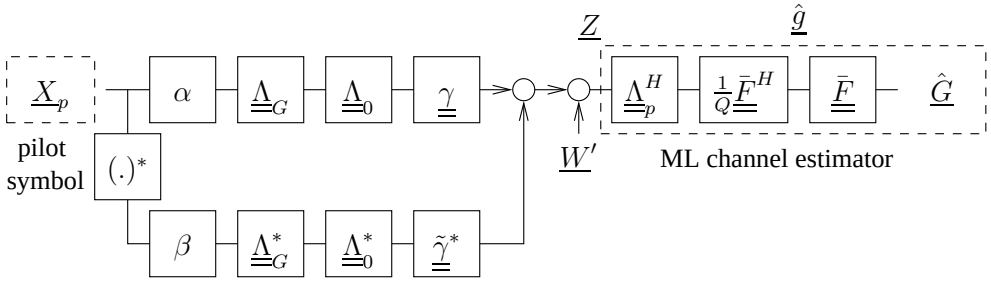

Fig. 4. Channel estimation.

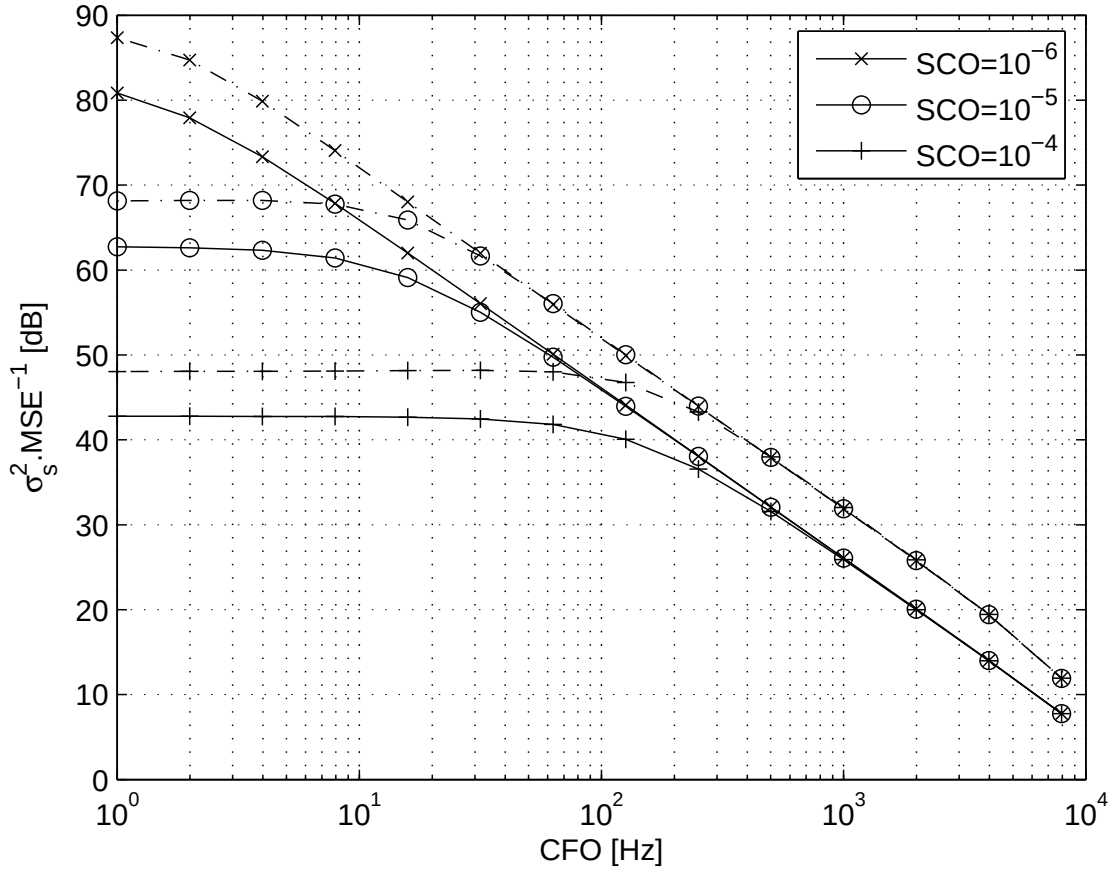

Fig. 5. Impact of CFO on MC-CDMA detection MSE for different SCO values (solid lines: impact of CFO/SCO; dashed lines: impact of channel estimation errors due to CFO/SCO).

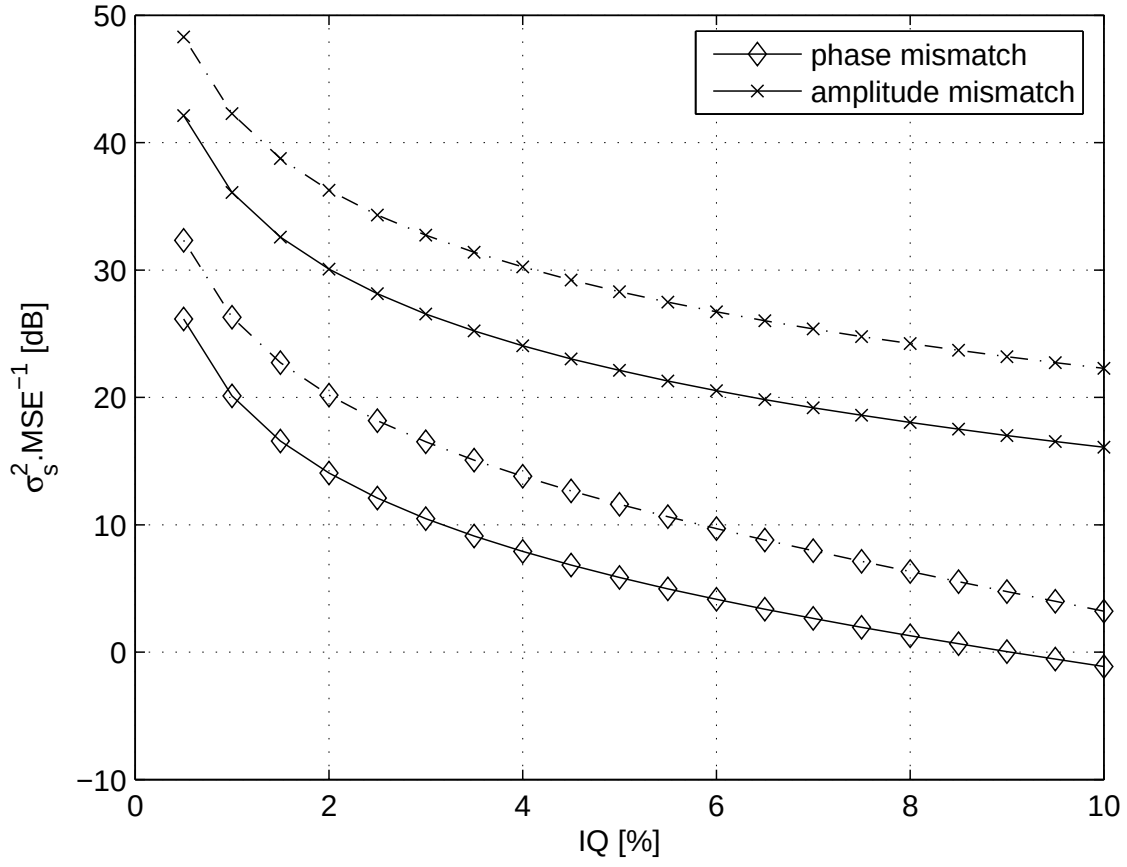

Fig. 6. Impact of IQ imbalance on MC-CDMA detection MSE (solid lines: impact of IQ imbalance; dashed lines: impact of channel estimation errors due to IQ imbalance).

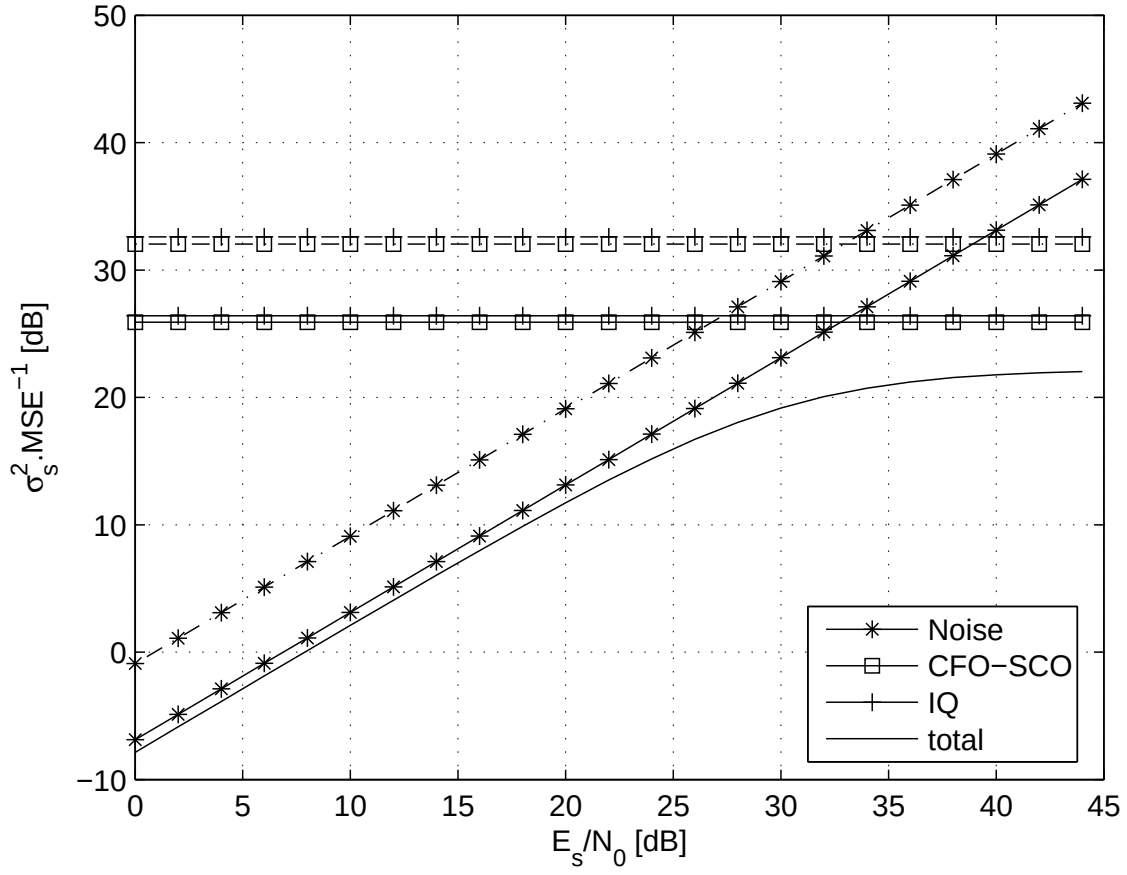

Fig. 7. Impact of non-idealities on MC-CDMA detection MSE (solid lines: impact of non-idealities, dashed lines: impact of channel estimation errors due to non-idealities).

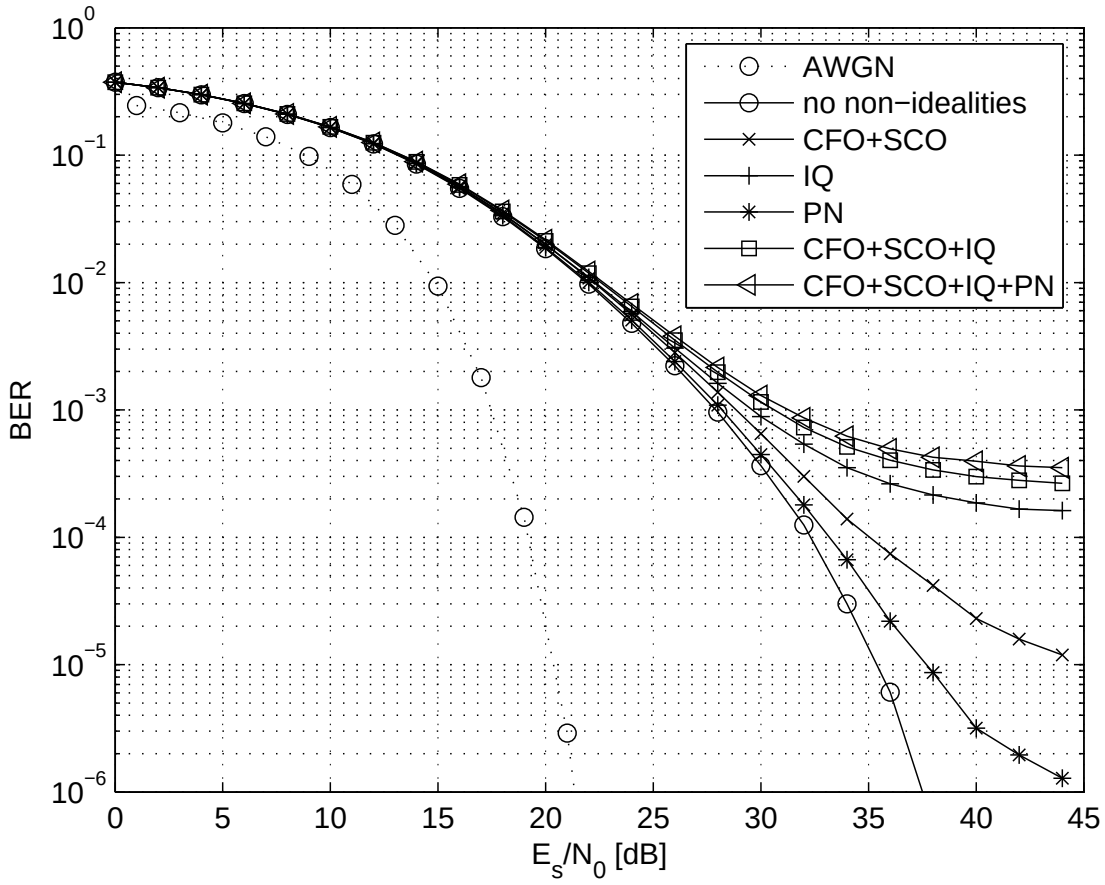

Fig. 8. Impact of each non-ideality on BER, 16QAM, static system.

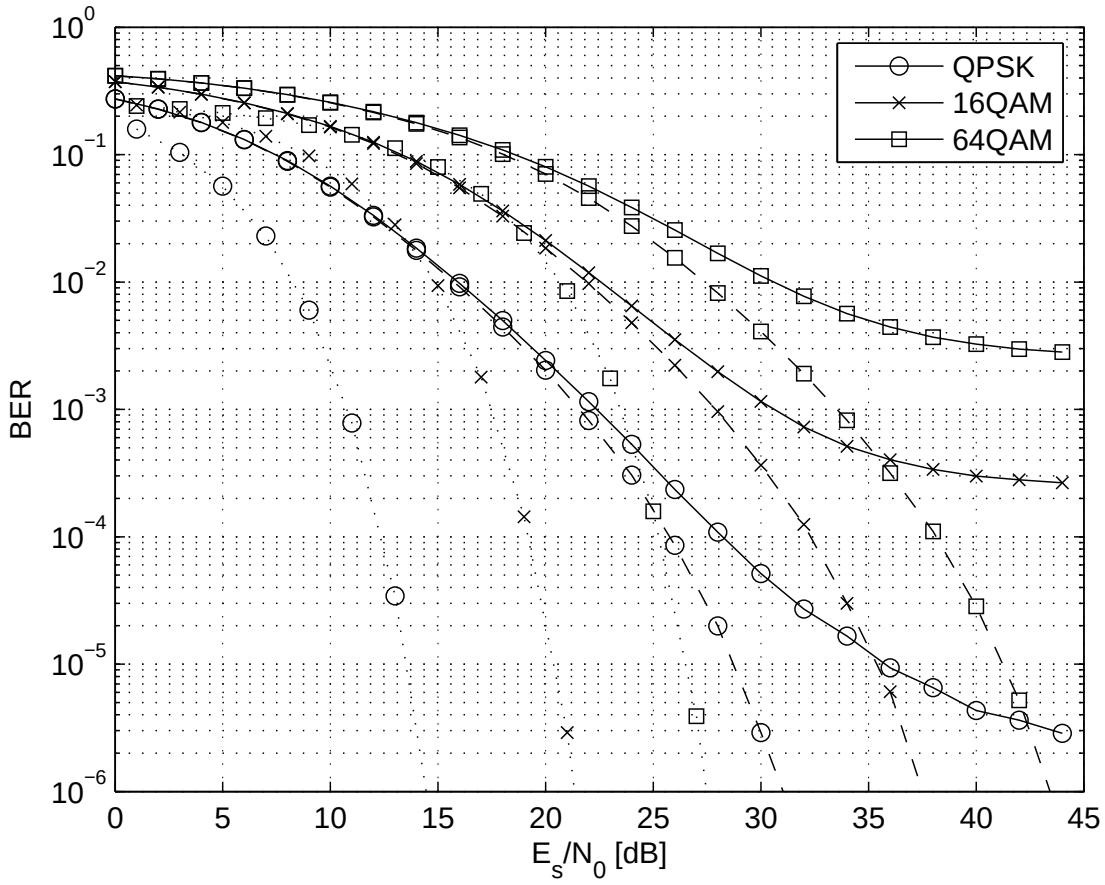

Fig. 9. Impact of the non-idealities on BER, static system (dotted lines: AWGN curves; dashed lines: ideal system, solid lines: system in the presence of non-idealities).

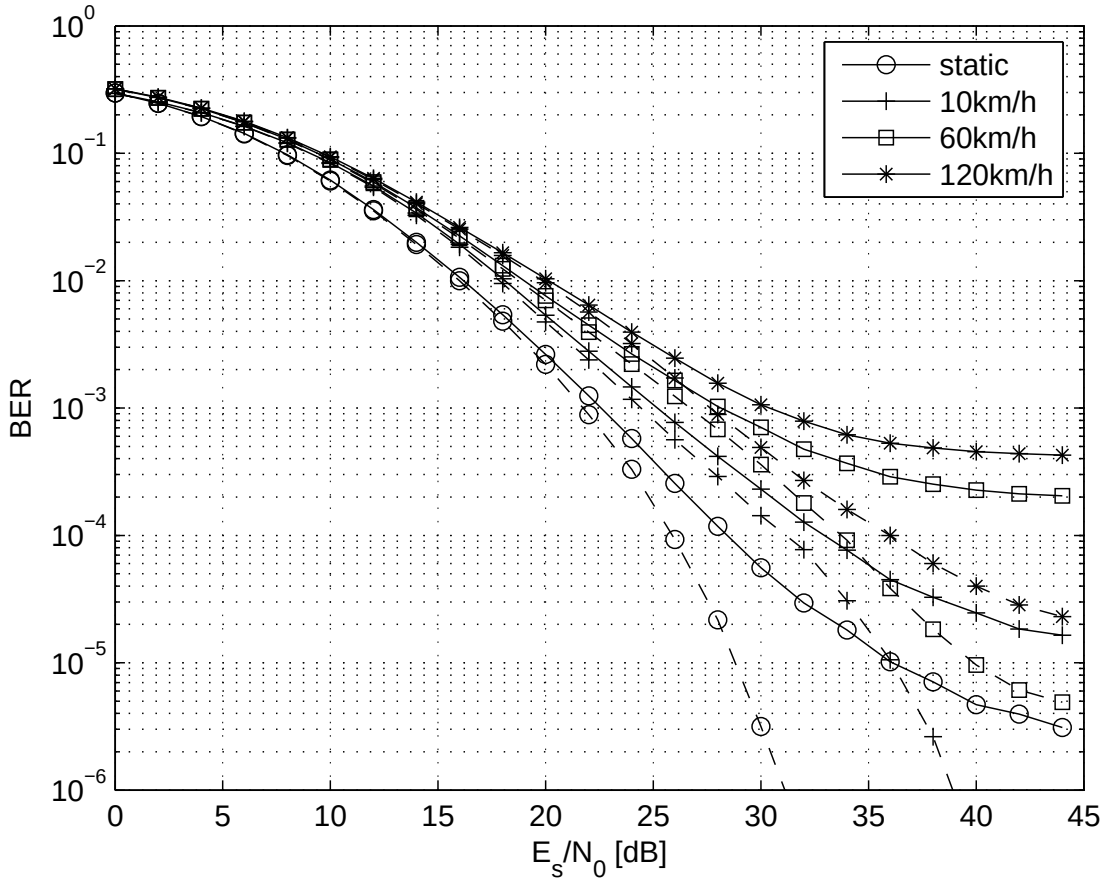

Fig. 10. Impact of the non-idealities on BER, QPSK (dashed lines: ideal system; solid lines: system in the presence of non-idealities).